Magnetism of small Fe clusters on Au(111) studied by x-ray magnetic circular dichroism

P. Ohresser* and N. B. Brookes
European Synchrotron Radiation Facility, Boîte Postale 220, 38043 Grenoble Cedex, France
and LURE, UMR 130, Bâtiment 209D, Boîte Postale 34, F-91898 Orsay, Cedex, France

S. Padovani
Laboratoire de Cristallographie, UPR 5031 CNRS-Université Joseph Fourier, INPG, Boîte Postale 166, 38042 Grenoble Cedex 9, France

F. Scheurer and H. Bulou
Institut de Physique et Chimie des Matériaux de Strasbourg, UMR-7504, 23 rue du Loess, 67037 Strasbourg Cedex, France
(Received 26 April 2001; published 23 August 2001)

Epitaxial growth of Fe on a reconstructed Au(111) surface leads to the formation of self-organized fcc Fe dots and stripes with increasing coverage. Using the sensitivity of x-ray magnetic circular dichroism (XMCD) and sum rule analysis, the changes in the magnetic properties in the low thickness range from ~0.1% of a monolayer (ML) to 4 ML, covering the unidimensional (1D) coalescence around ~0.3 ML and the two-dimensional percolation limit around ~1 ML have been determined. The evolution of the spin moment (m_{spin}) as a function of the thickness is correlated to the morphological transition. In particular, m_{spin} increases sharply at the 1D coalescence, what is attributed to a transition from a low-spin to a high-spin magnetic phase. We also observe a flipping of the easy axis of magnetization at the 1D coalescence from in-plane to out-of-plane. This unusual behavior is ascribed to the strong in-plane relaxation of the Fe films due to the particular pseudomorphic growth of Fe on the reconstructed Au(111) surface.

DOI: 10.1103/PhysRevB.64.104429 PACS number(s): 75.70.Cn, 75.70.Ak, 78.70.Dm

I. INTRODUCTION

The constant demand for higher storage density in the magnetic device industry has resulted in an increasing interest in systems with reduced dimensionality, such as ultra-thin magnetic films, and more recently, wires and dots.[1] For application purposes, strong magnetization, and long-range magnetic order at room temperature are needed. Interesting metastable magnetic states with controllable anisotropy are sought by adjusting the structure and/or the morphology (dimensionality) of the objects. Epitaxial fcc-type Fe structures grown on various Cu surfaces have shown a large variety of new magnetic phases depending on their intimate structure and morphology.[2–5]

In this context we have studied by means of x-ray magnetic circular dichroism (XMCD) the magnetic properties of Fe dots, organized on the Au(111) surface reconstruction. Using the sum rules[6,7] the orbital (m_{orb}) and spin (m_{spin}) magnetic moments are determined for clusters of several hundred atoms. The gold surface reconstruction[8] allows a very particular growth of a number of metals [e.g., Fe,[9–13] Co,[14] Ni,[15] Rh (Ref. 16)]. In the case of Fe, small single-layer high islands grow on the elbows of the herringbone surface reconstruction of Au(111) at room temperature, and form a regular array of islands, whose lateral size can be adjusted by varying the deposited amount of Fe.[9–11] This system is interesting from two points: First, it enables the control of the dimensionality; the Fe islands (0D) are well separated at low coverage, then coalesce to form parallel rows (1D) and eventually a connected 2D film.[9] Second, below 2 or 3 monolayers (ML), the growth is thought to be pseudomorphic[10,13] and hence, the in-plane lattice spacing of Fe is strongly expanded (~12% with respect to the normal nonmagnetic high-temperature fcc Fe phase). Above ~3 ML, the Fe film transits towards a bcc(110) structure.[9,10,12,13] As known from theoretical calculations, the magnetism of the Fe fcc phase is strongly dependent on the atomic volume, and therefore might give raise to unusual magnetic phases.[17–19] In this paper, the magnetic measurements are concentrated on the fcc phase, below ~3 ML. We show that below the 1D coalescence, surprisingly, the anisotropy is in-plane. A ''low-spin'' phase with a spin moment of about $1.4\mu_B$ is found. After the 1D coalescence the anisotropy is out-of-plane, as known from previous studies.[12,13] The spin moment increases to about $2.4\mu_B$. Above 3–4 ML, the spin and orbital moments show bulk bcc values. These results are discussed and compared to the ones obtained on vicinal Cu(111).[5]

II. EXPERIMENT

The experiment was carried out at beamline ID12B of the European Synchrotron Radiation Facility in Grenoble, using a 90% circularly polarized light from a helical undulator.[20] The magnetic characterization and the thin film growth were performed *in situ* by XMCD in an ultrahigh-vacuum chamber (5×10^{-11} mbar) containing the 7 T superconducting magnet and the Fe evaporation cell (the calibration procedure is described in Ref. 5). The technique is sensitive down to a fraction of a monolayer, as already demonstrated in the case of Fe deposited on a stepped Cu(111) surface.[5] For the low coverages the Fe films show a superparamagnetic behavior,[21] similar to Co on Au(111).[22–25] The islands behave as giant fluctuating spin blocs, which can be frozen below the blocking temperature T_B. The magnetic moments have to be measured below the T_B, on a saturated sample.

The blocking temperatures vary from about 200 down to 20 K, going from ~0.8 ML to the lowest coverages, and the saturation fields (measured at ~10 K) from about 0.2 to 2.5 T. The blocking temperatures are estimated by recording XMCD magnetization cycles as a function of applied field.[5] Therefore, the measurement temperature range went from 6 to 300 K. The applied magnetic field is aligned with the photon propagation vector and spin direction. By rotating the sample by an angle γ, it can be magnetized from out-of-plane to in-plane geometry allowing angular-dependent measurements. The sample preparation, consisting of Ar^+ sputtering and annealing (~900 K) cycles was done in a connected chamber. The presence of the Au surface reconstruction was checked with low energy electron diffraction (LEED), which exhibited the characteristic $(22\times\sqrt{3})$ pattern. Once clean, the sample was transferred, without breaking the vacuum, to the main chamber for Fe deposition and analysis.

III. RESULTS

The XMCD measurements are based on the circular magnetic dichroism at the Fe $L_{2,3}$ absorption edges. When the photon energy is swept across the spin-orbit split L_2 and L_3 edges $2p$ core electrons are excited into unoccupied $3d$ valence states. The spin conservation in the absorption process aligns the spin of the $2p$ core hole with that of the empty $3d$ orbitals. Strong spin-orbit coupling in the core shell leads to an x-ray absorption spectroscopy (XAS) signal which depends on the relative alignment of photon spin and sample magnetization. The XAS spectra were taken by measuring both the total electron yield and the total fluorescence yield (detected at 90° to the incident beam), although only the former is generally directly proportional to the absorption cross section.[26] The XMCD spectrum is the difference between the two XAS spectra recorded with opposite orientation of the magnetic field and the helicity of the light, which we will call μ_+ and μ_- for simplicity. μ_+ (μ_-) corresponds to the absorption coefficient of left- (right-) circularly polarized light, taking the direction of the magnetic field as the quantization axis. An example of a XMCD spectrum for 0.08 ML measured at normal incidence is given in Fig. 1.

Two important magneto-optical sum rules have been derived to deduce the orbital and spin magnetic moment from the XMCD.[6,7] Using the same notation as Ref. 27 one has for the $L_{2,3}$ edges

$$m_{\mathrm{orb}} = -\frac{4qN_h}{3r}, \tag{1}$$

$$m_{\mathrm{spin}}^{\mathrm{eff}} = -\frac{(6p-4q)N_h}{r}, \tag{2}$$

where p and q are, respectively, the integrals over L_3 and over (L_3+L_2) of the XMCD signal (given by $\mu_+-\mu_-$), r is the integral of the "white line" intensity of the magnetization-averaged absorption cross section $(\mu_++\mu_-)$ (to separate the "white line" from the continuum a simple steplike function was subtracted[5]), N_h is the number of holes

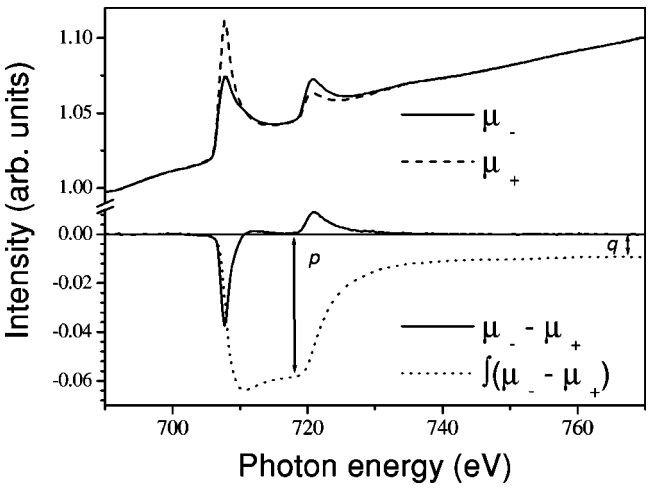

FIG. 1. Typical XMCD spectra for a coverage of 0.08 ML of Fe/Au(111) (total electron yield mode).μ_+ and μ_- correspond, respectively, to the absorption coefficient of left- and right-circularly polarized light (taking the direction of the magnetic field as the quantization axis). The spectra were recorded at normal incidence ($\gamma=0°$), $T=10$ K and $H=\pm 5$ T. The variable p and q on the integrate XMCD signal indicate the values used in the sum rules (see text for details).

in the $3d$ band. $m_{\mathrm{spin}}^{\mathrm{eff}}$ is the effective magnetic spin moment. It includes a dipolar term m_T describing the anisotropy of the spin moment

$$m_{\mathrm{spin}}^{\mathrm{eff}} = m_{\mathrm{spin}} - 7m_T. \tag{3}$$

Since the coverage range studied here is below 3 ML, there is no need to correct the data for saturation effects.[28] N_h is in principle unknown although it can be estimated from band structure calculations. In the case of bcc Fe, a value close to 3.39 gives a good agreement between theory and experiment.[27] However, since very small fcc structures are considered here, we will mostly consider magnetic moments per hole, i.e., m_{orb}/N_h and $m_{\mathrm{spin}}^{\mathrm{eff}}/N_h$, although N_h is not expected to vary a lot. For a given coverage, the incidence angle γ, i.e., the angle between the incident light and the surface normal, was varied from 0° to 60° in 15° steps. For each geometry we apply the sum rules on the measured XMCD spectra. The orbital magnetic moments measured perpendicular ($m_{\mathrm{orb}}^{\perp}$) and parallel ($m_{\mathrm{orb}}^{//}$) to the easy axis of magnetization are deduced by fitting the angular dependence of the orbital magnetic moment measured at the angle γ ($m_{\mathrm{orb}}^{\gamma}$). It is assumed that there is no anisotropy within the surface plane, what seems reasonable for fcc(111) oriented structures. Hence, using Bruno's model one has[29]

$$m_{\mathrm{orb}}^{\gamma} = m_{\mathrm{orb}}^{\perp} + (m_{\mathrm{orb}}^{//} - m_{\mathrm{orb}}^{\perp})\sin^2\gamma. \tag{4}$$

Similarly, to separate the dipolar and the spin contribution from $m_{\mathrm{spin}}^{\mathrm{eff}}$ given by the sum rule we follow the arguments of Stöhr and König[30] and suppose that the angular dependence of $m_{\mathrm{spin}}^{\mathrm{eff}}$ is entirely contained by m_T. One has

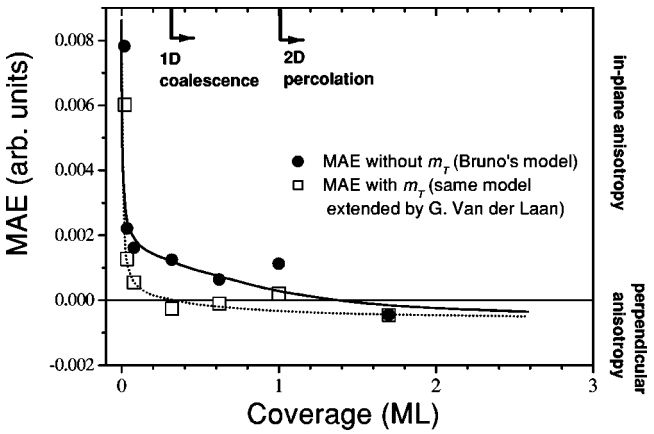

FIG. 2. MAE as a function of coverage. The solid circles corresponds to the model developed by Bruno (Ref. 29), and the open square to the model proposed by van der Laan (Ref. 31) which take into account the dipolar interaction (see text for details). The lines are guides for the eyes.

$$m_{\mathrm{spin}}^{\gamma-\mathrm{eff}}=(m_{\mathrm{spin}}-7m_T^{\perp})+\frac{21}{2}m_T^{\perp}\sin^2\gamma. \tag{5}$$

Fitting the angular dependence of $m_{\mathrm{spin}}^{\mathrm{eff}}$ allows us to extract m_{spin}. Bruno's model assumes a completely filled majority band. This is, however, not the case for fcc Fe and therefore, Van der Laan extended Bruno's model for partially filled bands.[31] The magnetocrystalline anistropy energy (MAE) is then no longer proportional to the anisotropy of the orbital momentum ($m_{\mathrm{orb}}^{\perp}-m_{\mathrm{orb}}^{//}$) and one has to take separately into account the orbital moments of the spin up and down bands. However, it is not possible with XMCD to obtain the contribution of the orbital moments separated by spin and for our purpose we only extend the commonly use Bruno's model with the dipolar contribution. Hence

$$\mathrm{MAE}\approx-\frac{1}{4}\xi(m_{\mathrm{orb}}^{\perp}-m_{\mathrm{orb}}^{//})+\frac{\xi^2}{\Delta E_{\mathrm{ex}}}\left[\frac{21}{2}\frac{3}{2}m_T^{\perp}+a\right], \tag{6}$$

where ξ is the spin orbit coupling, ΔE_{ex} the effective exchange between majority and minority bands (for Fe $\xi=0.05$ eV and $\Delta E_{\mathrm{ex}}\sim 3$ eV), and a is a term independent of the spin direction and gives only an energy shift. It is expected to be small and will be neglected.[32] Hence, only the dipolar contribution is taken into account here. It has to be mentioned that XMCD, either in the usual geometry, or in the transverse geometry (which provides the orbital moment anisotropy in a more direct way[33–35]) tends to overestimate the MAE.[36] In Ni/Pt multilayers for example, the MAE is 20 times smaller than the orbital momentum anisotropy as determined by XMCD.[37] Here, the MAE is discussed only in terms of relative changes of the magnetization easy axis orientation. The MAE is therefore given in arbitrary units. We also recall that XMCD is only sensitive to the magnetocrystalline anisotropy and does not take into account the shape anisotropy. The magnetocrystalline anisotropy energy deduced from the XMCD measurements is plotted in Fig. 2, using both models. The open squares and the full circles are

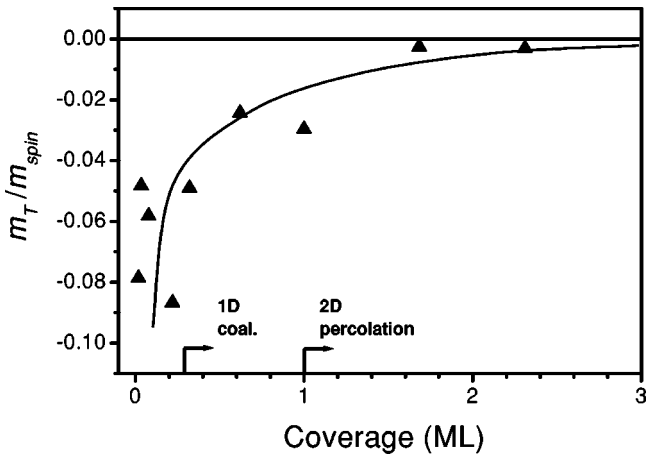

FIG. 3. Ratio m_T/m_{spin} as a function of coverage. The solid line is a guide for the eyes. The arrows on the top scale at 0.3, 1, and 3 ML correspond respectively to the approximate coverage where the Fe starts to coalesce into 1D wire, reaches the 2D percolation and undergoes the fcc to bcc phase transformation.

obtained by applying respectively Bruno's model[29] and the more recent Van der Laan one.[31]

One can see that the overall shape of the MAE is the same for both models. The magnetization is in-plane below a critical thickness, and turns to out-of-plane above, in both models. In the Van der Laan model however, the critical thickness is shifted towards a lower coverage, ~ 0.3 ML, instead of ~ 1.2 ML for the Bruno model, because of the dipolar contribution. Our experiments show that, if the effect of m_T can be neglected above ~ 2 ML, as is commonly assumed, it becomes sizeable and cannot be neglected anymore in the low thickness range. Indeed, Fig. 3 shows that m_T can reach 8% of m_{spin}, representing one third of the contribution to $m_{\mathrm{spin}}^{\mathrm{eff}}=m_{\mathrm{spin}}-7m_T$.

The variations of m_{spin}/N_h and m_{orb}/N_h are plotted in Fig. 4 as a function of Fe coverage. For bcc Fe films, i.e., for coverages above ~ 3 ML, typical bulk values are obtained for m_{spin}/N_h and m_{orb}/N_h (dashed lines) with a deduced spin moment of about $m_{\mathrm{spin}}\approx 2.1\mu_B$ (assuming $N_h=3.39$). One can notice a large increase of m_{orb}/N_h when moving from higher towards lower coverages, whereas for m_{spin}/N_h, two magnetic spin phases can be distinguished: Below the 1D coalescence (~ 0.3 ML) one has $m_{\mathrm{spin}}/N_h\approx 0.43\mu_B$/hole and once the 1D coalescence is completed, m_{spin}/N_h jumps to about $0.70\mu_B$/hole.

IV. DISCUSSION

To explain the magnetic behavior of Fe/Au(111) in the low thickness range (below 3 ML), one has to examine carefully the first stages of the growth mode of Fe at room temperature on Au(111). The Fe atoms diffuse and nucleate preferentially at the point defects of the gold herringbone reconstruction, where they form monatomic islands, with triangular and polygonal shapes.[9,10,38] They are arranged on a more or less regular array of 7.5 nm$\times$15 nm. The lateral size in the clusters, hence the number of atoms, is directly related to the amount deposited. Below about 0.3 ML, the

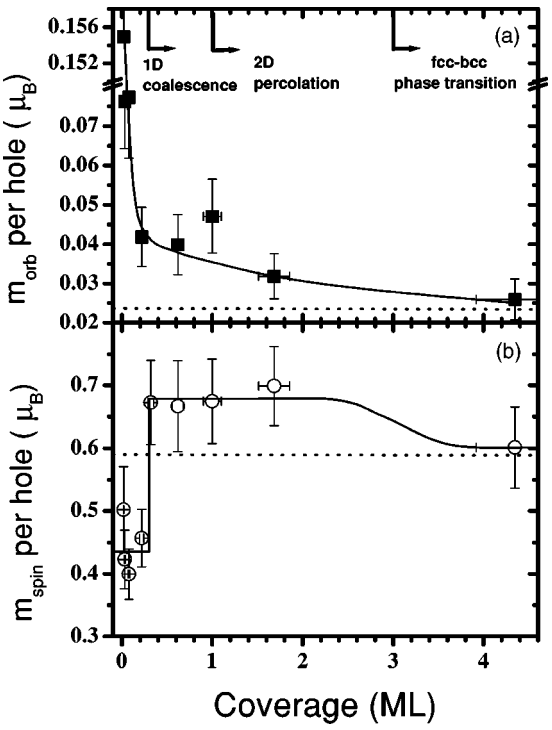

FIG. 4. Orbital (a) and spin magnetic moments (b) per hole, as a function of coverage. The solid lines are a guide for the eyes. The dashed lines correspond to the values for the bulk bcc Fe magnetic moment. The arrows on the top scale at 0.3, 1, and 3 ML correspond, respectively, to the approximate coverage where the Fe starts to coalesce into 1D wire, reaches the 2D percolation and undergoes the fcc to bcc phase transformation. All the measurements have been performed below the blocking temperature with a magnetic field sufficient to saturate the sample.

clusters remain separated. At 0.3 to 0.4 ML, the clusters reach a lateral size of 7.5 nm, so that adjacent clusters in a row (along a $[11\bar{2}]$ direction) come into contact, forming chainlike structures.[9,10,38] This growth stage is referred to as 1D coalescence in the discussion. Upon further deposition, additional clusters nucleate in-between the rows, interconnecting adjacent rows. Eventually, at ~ 1 ML, a coalesced 2D film is obtained and the second layer starts growing. The Fe film has an fcc structure up to about 3 ML, the thickness at which it undergoes a structural transition of the whole film towards the stable bcc(110) phase.[9,13,39] It is known from previous experiments that this structural phase transition induces a magnetization reorientation from out-of plane to in-plane.[39] However, the presence of an in-plane magnetization at very low thicknesses has never been mentioned. For submonolayer coverages, there are no precise structural data but from STM measurements, Fe is expected to grow pseudomorphically, that means with an in-plane lattice expansion of about 12%,[10] with respect to its high temperature nonmagnetic fcc phase.

The presence of a strong in-plane anisotropy for the lowest coverages is quite surprising. The switching from an in-plane to a perpendicular anisotropy is unusual since the surface anisotropy generally tends to favor the perpendicular geometry. However, strain effects, as observed for thicker Ni films on Cu(100) can be at the origin of spin reorientation transitions.[40,41] On another hand, when reducing the dimensions of the clusters, the symmetry breaking induced at the borders of the clusters may lead to an enhanced Néel-type surface or, in this case ''border'' anisotropy. Indeed, the in-plane anisotropy is observed below the 1D coalescence, when the Fe clusters remain isolated. It is clear that below 0.3 ML, there is a high proportion of edge atoms, resting in low-symmetry sites, which have high dipolar (m_T) and orbital (m_{orb}) contributions, as seen in Figs. 3 and 4(a). The increase of m_{orb} towards the lower coverages is also observed for Fe ''wires'' grown on vicinal Cu(111),[5] although it is by a factor of 6 here, whereas it is only a factor 2 in Fe/Cu(111)-vic, with respect to bcc Fe. Since the orbital momentum is quenched in bulk $3d$ materials, one is tempted to attribute the increase of m_{orb} to the reduced coordination. The cluster size and shape for a given coverage being known from the STM data, one can estimate the proportion of edge atoms. Assuming two types of atoms, central atoms in a cluster and edge atoms, leads to an orbital momentum of roughly $0.5\mu_B$ for an Fe edge atom on Au(111). Surprisingly, this value is the same as the one found for Fe/Cu(111)-vic when making the same estimation of the proportion of edge atoms. The nucleation density is much higher in the case of Fe/Au. A more precise estimation shows that there are about three times more edge atoms for Fe clusters on Au(111) than on Cu(111)-vic at similar coverages, what may explain the factor of three between the average values of the orbital moments for Fe clusters on Au(111) and Cu(111)-vic.

At the 1D coalescence, the proportion of edge atoms is drastically reduced, and there might be a modification in the strain due to the coalescing clusters. We tentatively attribute the magnetization reorientation at 0.3 ML to one or both effects. Due to the very complex structure of the reconstructed gold surface, the Fe atoms are located in many different symmetry sites. Unfortunately, this makes first principles calculations of the magnetic properties (anisotropy, phase and spin moment) of Fe on reconstructed Au(111) extremely difficult. We can therefore only try to give some reasonably possible mechanisms of our findings through very simplified considerations. To illustrate the border effect, we calculated in a Néel pair interaction model[42] the anisotropy energy of epitaxial Fe clusters on the herringbone-reconstructed Au(111) surface as a function of coverage (i.e., cluster size).

In the framework of this model, the magnetic energy W is written as a sum of elementary energy of magnetic interaction between pairs of nearest neighbor atoms

$$W = \frac{1}{2} \sum_{i,j} \omega_{ij}, \tag{7}$$

with

$$\omega_{ij} = \sum_{n=1}^{+\infty} g_{2n}(r_{ij}) P_{2n}(\cos \phi_{ij}), \tag{8}$$

where

$$g_n(r) = (l_n + m_n \delta r) \tag{9}$$

and

$$\delta r = r - r_0. \tag{10}$$

ϕ_{ij} is the angle between the magnetic moment on nearest neighbor sites i and j, and the interatomic distance $\vec{r}_{ij}$; g_n is a function depending only on the distance between the two atoms i and j,and P_n is a Legendre polynomial describing the angular dependence of the pair energy with respect to ϕ_{ij}. Terms of order higher than 2 are usually neglected. The microscopic coefficients l_2 and m_2 are linked to the magnetoelastic coefficients B_1 and B_2:

$$l_2 = \frac{3}{2} B_1, \tag{11}$$

$$m_2 = \frac{3}{2r_0}(3B_2 - B_1). \tag{12}$$

For bulk bcc iron $B_1 = -253\mu$ eV atom^{-1}, $B_2 = 556\mu$ eV atom^{-1} (Ref. 43), and $r_0 = 2.48$ Å, so $l_2 = -379.5\mu$ eV atom^{-1} and $m_2 r_0 = 2881.5\mu$ eV atom^{-1}. It is interesting to note that in the case of bulk Fe, l_2 and m_2 are of opposite sign. It means that the function $g_2(r)$ vanishes for a critical interatomic distance of

$$r = r_c = r_0\left(1 - \frac{B_1}{3B_2 - B_1}\right) = 2.807 \text{ Å}. \tag{13}$$

As a consequence, if the interatomic distance $r < r_c$, $g_2(r)$ is negative and then the easy magnetization axis is lined up with the interatomic direction $\vec{r}_{ij}$, while if $r > r_c$, $g_2(r)$ is positive and then the easy magnetization axis is perpendicular to the interatomic direction $\vec{r}_{ij}$. The Néel model intrinsically assumes that $g_2(r)$ is independent of the local symmetry. However, there is no reason that on the border of a cluster $g_2(r)$ has the same value as in its center or as in the bulk. Therefore, we extended the model to allow different values for the border and the center of a cluster. We introduce scaling factors, $C_{n_i m_j}$ in the pair interaction term ω_{ij}. n_i and m_j represent the number of nearest neighbors atoms located at sites i and j, respectively. Thus, the magnetic energy of the system is

$$W = \frac{1}{2}\sum_{i,j}\sum_{n=1}^{6}\sum_{m=1}^{6} C_{nm} g_2(r_{ij}) P_2(\cos\phi_{ij})\,\delta_{n,n_i}\delta_{m,m_j}. \tag{14}$$

The gold surface and its reconstruction are represented in Fig. 5. The positions of the gold atoms for the reconstructed surface are obtained by molecular dynamics simulations.[44] As mentioned above, there are strong inhomogeneities in the nearest-neighbor distances on the gold surface: Whereas the bulk nearest neighbor distance is 2.88 Å, it drops to about 2.82–2.85 Å on the fcc or hcp parts (areas I and II on Fig. 5) of the surface, to 2.78 Å in the discommensuration lines (area III on Fig. 5), down to ~2.72 Å in the vicinity of the kinks (area IV on Fig. 5).[44] The lower lattice parameter at the surface comes from a densification of ~4% of the gold surface.

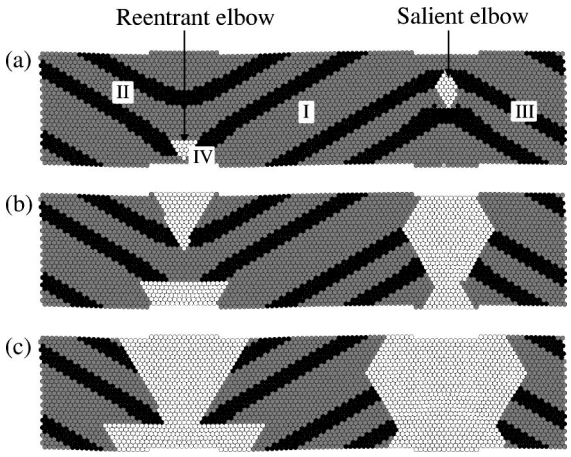

FIG. 5. Fe/Au(111): (a) 0.02 ML, (b) 0.20 ML, and (c) 0.44 ML. The gray atoms of the zone I and II represent, respectively, the fcc ($r \sim 2.85$ Å) and hcp ($r \sim 2.82$ Å) coherent epitaxial areas, the black atoms of the zones III and IV represent, respectively, the discommensuration lines ($r \sim 2.78$ Å) and the kinks ($r \sim 2.72$ Å). The iron clusters are represented by white atoms.

The STM pictures in the literature allow us to simulate the position and an average shape of the clusters on the surface. Two types of nucleation sites are activated for room temperature deposition: the reentrant and salient elbows of the reconstruction. On the reentrant elbow sites, triangular clusters are formed, while they are diamond-shaped on the salient elbows. A perfect ''local'' pseudomorphy is supposed for the calculation, in agreement with STM data.[10]

It is amazing that the nearest-neighbor distances are spread around 2.80 Å, which corresponds exactly to the critical separation of r_c at which the pair interaction undergoes a sign change. This roughly means that, when the clusters are small (i.e., the atoms are located in the vicinity of the kinks), their nearest-neighbor distance being below 2.80 Å, an in-plane anisotropy is favored. When the clusters grow in size, they grow on the fcc or hcp parts, having nearest neighbor distances above r_c, which favors an out-of plane anisotropy.

The full line in Fig. 6 shows the calculated magnetic anisotropy energy as a function of coverage together with the experimental data, assuming a bulk value for l_2 and m_2, for all sites. The only adjustable parameter is the scaling factor of the MAE, since XMCD does not give absolute values (see Sec. III). Allowing different values for edge and central pairs improves the agreement with the data points but does not change the overall shape, which is already obtained taking bulk values for all pairs. For the dashed and dotted curves (see caption) we assumed that

$$C_{nm} = \begin{cases} C^{\text{edge}} & \text{if } (n,m) \in [1,5], \\ C^{\text{center}} & \text{if } n = m = 6. \end{cases} \tag{15}$$

Between 0 and 0.02 ML, there is a rapid increase of the

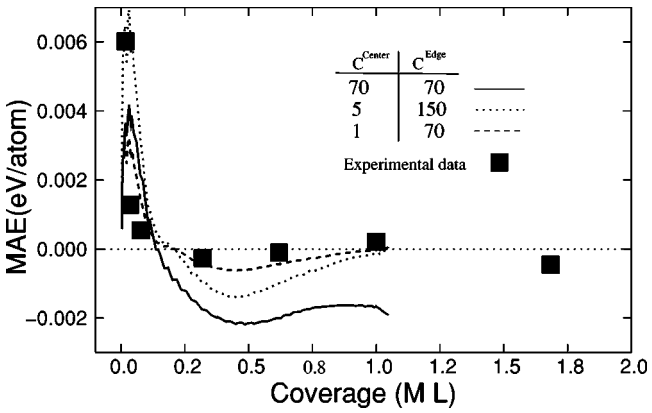

FIG. 6. Calculated and experimental MAE. The shape of the clusters is shown on Fig. 5.

MAE. Its origin lies in the fact that the nucleation begins at the edge dislocation [Fig. 5(a)]. In these areas, the nearest neighbors distances are about 2.75 Å; thus in-plane easy magnetization axis orientation is the most favorable situation from an energetic point of view.

From 0.02 to about 0.20 ML, the MAE decreases and changes sign, explaining the observed reorientation of the magnetization. From 0.20 to ~0.4 ML, the out-of plane anisotropy gets stronger. In this range, the clusters stretch over the coherent epitaxial area where the nearest neighbors distances are about 2.85 Å [Fig. 5(b)], thus favoring perpendicular anisotropy. At 0.4 ML, the iron clusters located on the reentrant elbows coalesce, and the growth continues on the discommensuration lines [Fig. 5(c)], which induces a decrease of the MAE .

We emphasize that although this model may describe qualitatively the anisotropy of this system as a function of coverage, one must be aware that, first, the hybridization with the substrate is completely ignored (it is known that this latter may play an important role[45]), and second, the magnitude of the pair interaction (or equivalently the magnetoelastic coefficients) is assumed to be identical to the one in a bulk environment although the value of g_2 for the border atoms and for central atoms are probably not the same, and different from the bulk value. An ''artificial'' increase of g_{edge} with respect to g_{center} improves the fit between our experimental data and the calculated ones in the Néel model. A more detailed theoretical analysis of this latter point will be published in a forthcoming paper.

Although it appears from these experiments that there is a strong influence of the dimensionality (reduced symmetry) on the orbital moment, it does not appear clearly that there might be any on the spin moment. The strain plays probably the major role on the spin moment. At the 1D coalescence, there is an abrupt spin phase transition (Fig. 4(b)). Taking $N_h=3.39$, one has $m_{\text{spin}}=(1.4\pm0.2)\mu_B$ below the coalescence and $m_{\text{spin}}=(2.4\pm0.2)\mu_B$, above. The magnetism of Fe is very sensitive to structural changes, and in particular to the atomic volume in the fcc phase. Slight variations of the lattice parameter may produce different phases and spin moments. For instance, ferrimagnetic, nonmagnetic, antiferromagnetic phases are predicted[17–19] and observed[39–41,45–47] depending on the very structure of Fe. The phase above 0.3 ML can be related to the high-spin fcc phase, which is also found on Fe/Cu(100) between 2 and 4 ML Fe (Refs. 48–50) (actually a tetragonalized fcc structure) and on Fe/Cu(111) for pulsed laser deposited Fe.[51,52] One has, however, to be careful, since the three systems are definitely not equivalent, neither from the structure, nor from the morphology. Nevertheless, the high spin phase obtained for Fe/Au(111) must be close to the one predicted for expanded fcc Fe, since the value of $m_{\text{spin}}=2.4\mu_B$ is in excellent agreement with the calculations.[17–19] Below 0.3 ML, however, there is a sharp transition towards a low-spin phase, which may be either a true low spin phase, or a noncompensated antiferromagnetic phase. The transition from low to high spin must be related to the structural or morphological changes at this growth stage. It is possible that there is a modification of the strain in the Fe islands, following the connection of the clusters into 1D wires at the coalescence. A similar spin phase transition is observed on Fe/Cu(111)-vic,[5] when isolated islands start to coalesce to chains along the steps of the vicinal surface. In this latter case, there is a transition from $m_{\text{spin}}=1.4\mu_B$ below the coalescence to $m_{\text{spin}}=0.7\mu_B$ above. Contrary to Fe/Au(111), the high spin phase is not observed, and the transition takes place between two low spin phases. Therefore, the structures of the small clusters must be different on both systems. At least the strain is different since the lattice mismatch is 12% in the case of Fe/Au(111), whereas it is 2.5% for Fe/Cu(111). The larger the volume expansion, the larger the spin moment is. On this basis, we attribute the high spin phase between 0.3 and 2–3 ML to the strongly expanded fcc structure. Because of the abruptness of the spin transition, we exclude alloying effects, which may also lead to modifications in the spin moment, although in the case of FeAu alloys, a large spin moment is expected ($\sim 2.2\mu_B$).[53–55]

Consequently the observed transition of the magnetic spin moment at the coalescence is ascribed to the high sensitivity of the Fe fcc phase to any structural changes. This is further demonstrated by recent XMCD studies on supported bcc-Fe clusters[56] and Co clusters grown on Au(111)[57] which show no effect on the spin moment at the coalescence.

V. CONCLUSION

Using XMCD, the quantitative magnetic properties of Fe deposited on a reconstructed Au(111) surface were investigated, from very small isolated and self-organized clusters, to coalesced chains and films. The variation of the spin and the orbital moment were analyzed as a function of coverage, which allowed us to control the size and dimensionality of the nanostructures. It seems that dimensionality effects play an important role on the orbital moment only. The most striking result is the observation of a low-spin phase with in-plane anisotropy below the 1D coalescence at 0.3 ML. The variations of the magnetic anisotropy are accompanied by a strong increase of both orbital and dipolar moments when reducing the coverage, attributed to the edge atoms in the

clusters. At 0.3 ML, there is a magnetic phase transition towards a high-spin phase which we attribute to a modification in the strain state upon coalescence, corresponding to a fcc Fe phase close to the theoretically predicted fcc high spin phase. For the lowest coverages, below the 1D coalescence the Fe is either in a low spin phase or ferrimagnetic phase with a small net spin moment.

ACKNOWLEDGMENTS

The authors are grateful to K. Larsson for his invaluable technical assistance. We also want to thank O. Fruchart for fruitful discussion and providing us with unpublished STM pictures. The potentials for the calculation of the gold surface were kindly provided by C. Goyhenex.

*Present address: LURE, Centre Universitaire Paris Sud, Bat. 209D, B.P. 34, F-91898 Orsay, France.

[1] *Ultrathin Magnetic Structures*, edited by J. A. C. Bland and B. Heinrich (Springer, Berlin, 1994).

[2] H. Jenniches, J. Shen, CH.V. Mohan, S. Sundar Manoharan, J. Bartel, P. Ohresser, M. Klaua, and J. Kirschner, Phys. Rev. B **59**, 1196 (1999), and references therein.

[3] J. Shen, R. Skomski, M. Klaua, H. Jenniches, S. Sundar Manoharan, and J. Kirschner, Phys. Rev. B **56**, 2340 (1997).

[4] J. Shen, M. Klaua, P. Ohresser, H. Jenniches, J. Barthel, Ch.V. Mohan, and J. Kirschner, Phys. Rev. B **56**, 11 134 (1997).

[5] P. Ohresser, G. Ghiringhelli, O. Tjernberg, N.B. Brookes, and M. Finazzi, Phys. Rev. B **62**, 5803 (2000).

[6] B.T. Thole, P. Carra, F. Sette, and G. van der Laan, Phys. Rev. Lett. **68**, 1943 (1992).

[7] P. Carra, B.T. Thole, M. Altarelli, and X. Wang, Phys. Rev. Lett. **70**, 694 (1993).

[8] J.V. Barth, H. Brune, G. Ertl, and R.J. Behm, Phys. Rev. B **42**, 9307 (1990).

[9] B. Voigtländer, G. Meyer, and N.M. Amer, Surf. Sci. Lett. **255**, L529 (1991).

[10] J.A. Stroscio, D.T. Pierce, R.A. Dragoset, and P.N. First, J. Vac. Sci. Technol. A **10**, 1981 (1992).

[11] D.D. Chambliss, K.E. Jonhson, R.J. Wilson, and S. Chiang, J. Magn. Magn. Mater. **121**, 1 (1993).

[12] G. Lugert, W. Robl, L. Pfau, M. Brockmann, and G. Bayreuther, J. Magn. Magn. Mater. **121**, 498 (1993).

[13] J. Xu, M.A. Howson, P. Hucknall, B.J. Hickey, R. Venkataraman, C. Hammond, M.J. Walker, and D. Greig, J. Appl. Phys. **81**, 3908 (1997).

[14] B. Voigtländer, G. Meyer, and N.M. Amer, Phys. Rev. B **44**, 10 354 (1991).

[15] W.G. Cullen and P.N. First, Surf. Sci. **420**, 53 (1999).

[16] E.I. Altman and R.J. Colton, Surf. Sci. Lett. **304**, L400 (1994).

[17] V.L. Moruzzi, P.M. Marcus, and J. Kübler, Phys. Rev. B **39**, 6957 (1989).

[18] Yu-mei Zhou, Wen-qing Zhang, Lie-ping Zhong, and Ding-sheng Wang, J. Magn. Magn. Mater. **145**, L273 (1995).

[19] E.G. Moroni, G. Kresse, J. Hafner, and J. Furthmüller, Phys. Rev. B **56**, 15 629 (1997).

[20] J. Goulon, N.B. Brookes, C. Gauthier, J.B. Goedkoop, C. Goulon-Ginet, M. Hagelstein, and A. Rogalev, Physica B **208&209**, 199 (1995).

[21] See, e.g., A.H. Morrish, *The Physical Principles of Magnetism* (Wiley, New York, 1965).

[22] H. Takeshita, Y. Suzuki, H. Akinaga, W. Mizutani, K. Ando, T. Katayama, A. Itoh, and K. Tanaka, J. Magn. Magn. Mater. **165**, 38 (1997).

[23] H.A. Dürr, S.S. Dhesi, E. Dudzik, D. Knabben, G. van der Laan, J.B. Goedkoop, and F.U. Hillebrecht, Phys. Rev. B **59**, R701 (1999).

[24] E. Dudzik, H.A. Dürr, S.S. Dhesi, G. van der Laan, D. Knabben, and J.B. Goedkoop, J. Phys.: Condens. Matter **11**, 8445 (1999).

[25] S. Padovani, I. Chado, F. Scheurer, and J.P. Bucher, Phys. Rev. B **59**, 11 887 (1999).

[26] V. Chakarian, Y.U. Idzerda, and C.T. Chen, Phys. Rev. B **57**, 5312 (1998).

[27] C.T. Chen, Y.U. Idzerda, H.-J. Lin, N.V. Smith, G. Meigs, E. Chaban, G.H. Ho, E. Pellegrin, and F. Sette, Phys. Rev. Lett. **75**, 152 (1995).

[28] R. Nakajima, J. Stöhr, and Y.U. Idzerda, Phys. Rev. B **59**, 6421 (1999).

[29] P. Bruno, Phys. Rev. B **39**, 865 (1989).

[30] J. Stöhr and H. König, Phys. Rev. Lett. **75**, 3748 (1995).

[31] G. van der Laan, J. Phys.: Condens. Matter **10**, 3239 (1998).

[32] G. van der Laan (private communication).

[33] H.A. Dürr and G. van der Laan, Phys. Rev. B **54**, R760 (1996).

[34] H.A. Dürr and G. van der Laan, J. Appl. Phys. **81**, 5355 (1997).

[35] H.A. Dürr, G.Y. Guo, G. van der Laan, J. Lee, G. Lauhoff, and J.A.C. Bland, Science **277**, 213 (1997).

[36] S.S. Dhesi, G. van der Laan, E. Dudzik, and A.B. Shick, Phys. Rev. Lett. **87**, 067201 (2001).

[37] F. Wilhelm, P. Poulopoulos, P. Srivastava, H. Wende, M. Farle, K. Baberschke, M. Angelakeris, N.K. Flevaris, W. Grange, J.-P. Kappler, G. Ghiringhelli, and N.B. Brookes, Phys. Rev. B **61**, 8647 (2000).

[38] O. Fruchart (private communication).

[39] C. Chappert, P. Bruno, B. Bartenlian, P. Beauvillain, A. Bounouh, R. Megy, and P. Veillet, J. Magn. Magn. Mater. **148**, 165 (1995).

[40] M. Farle, B. Mirwald-Schulz, A.N. Anisimov, W. Platow, and K. Baberschke, Phys. Rev. B **55**, 3708 (1997).

[41] O. Hjortstam, K. Baberschke, J.M. Wills, B. Johansson, and O. Eriksson, Phys. Rev. B **55**, 15 026 (1997).

[42] L. Néel, J. Phys. Radium **15**, 15 (1954).

[43] D. Sander, Rep. Prog. Phys. **62**, 809 (1999).

[44] H. Bulou and C. Goyhenex, Phys. Rev. B (to be published).

[45] J. Dorantes-Dávila and G.M. Pastor, Phys. Rev. Lett. **81**, 208 (1998).

[46] Keeyung Lee and J. Callaway, Phys. Rev. B **48**, 15 358 (1993).

[47] Ph. Kurz, G. Bihlmayer, K. Hirai, and S. Blügel, Phys. Rev. Lett. **86**, 1106 (2001).

[48] J.G. Tobin, G.D. Waddill, and D.P. Pappas, Phys. Rev. Lett. **68**, 3642 (1992).

[49] J. Thomassen, F. May, B. Feldmann, M. Wuttig, and H. Ibach, Phys. Rev. Lett. **69**, 3831 (1992).

[50] R. Allenspach and A. Bischof, Phys. Rev. Lett. **69**, 3385 (1992).

[51] J. Shen, P. Ohresser, Ch.V. Mohan, M. Klaua, J. Barthel, and J. Kirschner, Phys. Rev. Lett. **80**, 1980 (1998).

[52] P. Ohresser, J. Shen, J. Barthel, M. Zheng, Ch.V. Mohan, M.

Klaua, and J. Kirschner, Phys. Rev. B **59**, 3696 (1999).
[53] I. Galanakis, M. Alouani, and H. Dreyssé, Phys. Rev. B **62**, 6475 (2000).
[54] K. Takanashi, S. Mitani, M. Sano, H. Fujimori, H. Nakajima, and A. Osawa, Appl. Phys. Lett. **67**, 1016 (1995).
[55] K. Sato, E. Takeda, M. Akita, M. Yamaguchi, K. Takanashi, S. Mitani, H. Fujimori, and Y. Suzuki, J. Appl. Phys. **86**, 4985 (1999).
[56] M. Marangolo (private communication).
[57] P. Ohresser *et al.* (unpublished).